Measurement of Angular Vibrations in Rotating Shafts: Effects of the Measurement Setup Non-Idealities

Tommaso Addabbo, Ada Fort, Luca Pancioni,
Mauro Di Marco, Valerio Vignoli

Department of Information Engineering and Mathematical Sciences
University of Siena, 53100 Italy
(e-mail: addabbo@dii.unisi.it)

Roberto Biondi, Stefano Cioncolini

GE Oil & Gas, 50127 Florence, Italy

⋆ RESEARCH MANUSCRIPT ⋆

– PLEASE REFER TO THE PUBLISHED PAPER[1] –

Abstract

In this paper the authors discuss a measurement method, based on the zero-crossing demodulation technique of FM signals, to estimate the angular velocity vibrations of a rotating shaft. The demodulation algorithm is applied without any filtering to the direct voltage output issued by some probes sensing the passages of arbitrarily shaped targets installed on the rotating shaft. The authors discuss a theoretical approach to analyze the measurement problem taking into account the chief non-idealities related to the measurement set-up, i.e., they have investigated the effects of both the shaft side vibrations and the irregular shape of the targets. On the basis of the theoretical results the authors propose a measurement method that can reject the effects of these mentioned non-idealities, exploiting the measurements of two or more probes properly positioned around the shaft.

1 Introduction

The measurement of the angular velocity variations of a rotating shaft plays a key role in a broad range of fields and applications, from energy production with turbo-machines to the automotive industry. Among the measurement methods, probably the simplest one is to sense the passing of the teeth of a geared wheel

[1] Instrumentation and Measurement, IEEE Transactions on, 2013, vol. 62, n. 3, p. 532-543.

installed on the shaft, since the time-delay between the teeth is inversely proportional to the rotational speed. Exploiting this idea, some papers have been published in literature for specific targeted applications, but an overall theoretical approach to evaluate the accuracy of the measurement method has not been yet discussed exhaustively, even considering the most common measurement setup non-idealities [1–7]. The above mentioned papers deal with the problem of measuring the angular velocity of rotating shafts in specific applications, analyzing different aspects of the measurement task and adopting in most cases an heuristic and simplified point of view. In [6,7] some theoretical aspects were investigated, e.g., the estimation of measurement uncertainties.

Differently from the above mentioned works, in this paper the authors let the shape profile of the geared wheel have an irregular shape: for example, the 'geared wheel' can be represented by a bolted joint in the shaft, being the bolts representing 'teeth' whose geometrical profiles may differ from each others. When either fault diagnosis or predictive maintenance have to be performed on scarcely accessible or modifiable machineries, this measurement technique is often the only one available and a theoretical analysis of the accuracy of this method is of some interest, especially when referring to those applications in which the measurement precision represents a critical issue (e.g., the measurement of torsional vibrations in turbo-machines with extreme-stiff shafts [7–9]). For simplicity, regardless of the actual profile of the sensed profile, in the following the authors refer to a generic geared wheel, or cogwheel.

In this paper the authors extend the work presented in [10], providing a deep analysis of the effects on the measurement due to both the irregular cogwheel shape and the side shaft vibrations. As a result, they show that the well-known zero-crossing demodulation technique can represent a valid solution for retrieving the angular vibrational signal, and propose a method to increase the measurement accuracy by properly combining two or more probes.

Adopting a presentation organization similar to that one of [10], this paper is structured as in the following. In Sec.2 the authors introduce the notation and a reference probe physical model. In Sec. 3 the analytical representation of the probe voltage signal is discussed, showing that due to the shaft angular vibrations the signal can be written as an infinite summation of frequency-modulated sinusoidal components. In Sec. 4 the authors analyze the frequency spectrum of the probe output voltage, linking its spectral characteristics to the shape of the sensed geared wheel installed on the shaft, whereas in the Sec. 5 the effects of the shaft side vibrations are analyzed. In Sec. 6 the authors show how to estimate the vibrational signal using the zero-crossing technique, discussing a sensitivity analysis of the proposed measurement method. In Secs. 7 and 8 the authors propose a method to reject the effects of the irregular cogwheel profile and the shaft side vibrations, respectively. Conclusions and references close the paper.

All the examples shown in this paper are based on simulations. The use of simulations was necessary to evaluate the correctness of the theoretical approach, since simulations allow for setting up an a-priori known physical condition of the rotating shaft, including angular vibrations, shaft side vibrations and cogwheel shape. The general results presented in this paper were also validated by means of experimental measurements made at the GE Oil & Gas Facility in Florence, Italy. Also these results, not reported in this paper for conciseness sake, confirm the theoretical predictions discussed in the following Sections.

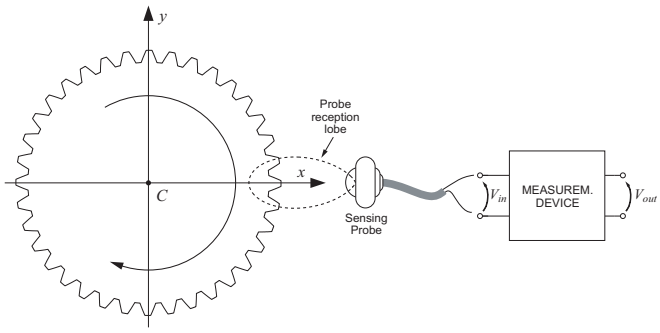


Figure 1: Illustration of a basic reference measurement setup.

2 Notation and Probe Physical model

In this work the authors refer to an arbitrarily shaped cogwheel (Fig. 1) installed on the shaft and positioned in front of a sensing probe. By denoting with $\omega(t)$ the instantaneous angular velocity of the cogwheel with respect to its center $\mathbf{C}$ (measured in rad/s), the measurement device in Fig. 1 is devised for measuring the variations of the shaft angular velocity with respect to its average value. The cogwheel center is assumed to be nominally placed in the origin, even if small vibrations (shaft side vibrations) are allowed: in such case, the positioning vector $\mathbf{C} = (C_x, C_y)$ is a function of time, i.e., $\mathbf{C}(t) = (C_x(t), C_y(t))$. From a practical point of view, the average angular velocity is calculated referring to a finite time-window of length W, and the angular variations are calculated as

$$\Delta\omega(t) = \omega(t) - \frac{1}{W}\int_{t-W}^{t} \omega(\tau)d\tau. \tag{1}$$

In the following, angular vibrations are managed as small perturbations of a constant rotating shaft with angular velocity ω_0, i.e.,

$$\omega(t) = \omega_0 + \tilde{\omega}(t) = \omega_0 + \Delta\omega_{\max} m(t), \tag{2}$$

where the term $\tilde{\omega}$ takes into account the angular vibrations, $\Delta\omega_{\max}$ is the maximum level of $|\tilde{\omega}|$ and $m(t)$ is non-dimensional, with zero mean value and $|m(t)| \leq 1, t \geq 0$.

2.1 Probe modeling

A probe is used to sense the teeth passages of the geared wheel installed on the shaft. Since the theoretical approach discussed in this paper does not refer to specific characteristics of the probe, in the following a generic model for the sensing probes is adopted. Accordingly, referring to Fig. 1, it is assumed that the probe has a spatial reception lobe symmetrical with respect to the x axis. Moreover, the probe reception profile is assumed to be described with a generic Gaussian single-lobe having normalized amplitude and -3dB half-angle θ_0, i.e,

$$f(\theta) = \sqrt{\frac{\ln 2}{\pi\theta_0^2}} e^{-\frac{\theta^2 \ln\sqrt{2}}{\theta_0^2}}, \qquad -\pi \leq \theta \leq \pi. \tag{3}$$

From an electrical point of view, the probe is modeled as a linear time-invariant system with generic band-pass transfer function

$$H(\omega) = \frac{jG\omega}{\left(1 + j\frac{\omega}{\omega_L}\right)\left(1 + j\frac{\omega}{\omega_H}\right)}. \tag{4}$$

In the above transfer function G is a gain factor taking into account the probe distance from the cogwheel, whereas $\omega_L \ll \omega_H$ are the two pulsations associated with the high-pass and low-pass cut-off frequencies.

3 Analytical representation of the probe signal

Referring to Fig.1, an analytical representation of the probe voltage signal V_{in} can be obtained following the approach discussed in this Section. The authors initially assume to deal with a shaft rotating in absence of side vibrations, that is, the cogwheel center $\mathbf{C}$ is hypothesized to be the fixed point $(C_x, C_y) = (0, 0)$. Moreover, the probe spatial reception lobe is assumed to be focused on a small, limited portion of the cogwheel profile, i.e, referring to Fig. 2,

$$\alpha_0 \ll \theta_0 \tag{5}$$

(the assumption typically makes sense, since $D \ll R$). By denoting with $r : [0, 2\pi) \to \mathbb{R}^+$ the polar representation of the cogwheel profile (with respect to the point $\mathbf{C}$), the authors note that under the assumption (5) the cogwheel profile can be *locally approximated* by the projection $r_y : \mathbb{R} \to \mathbb{R}^+$ of the polar representation r on the y axis, in front of the probe. In other words, the rotational motion of the cogwheel in front of the probe can be described as an equivalent relative motion of the probe along the y-axis, in front of the cogwheel 'unrolled' profile

$$r_y(y) = r\left(\frac{y}{R} \bmod 2\pi\right). \tag{6}$$

Since (6) is a periodic function with period $2\pi R$, it can be expressed as an infinite Fourier series

$$r_y(y) = \frac{a_0}{2} + \sum_{n=1}^{\infty}\left[a_n \cos\left(\frac{ny}{R}\right) + b_n \sin\left(\frac{ny}{R}\right)\right]. \tag{7}$$

By reordering the above series, eq. (7) can be rewritten in a more compact analytical form, as the infinite sum of cosines

$$r_y(y) = \sum_{p=0}^{\infty} A_p \cos(2\pi\xi_p\ y + \phi_p), \tag{8}$$

where

$$A_p = \begin{cases} \frac{a_0}{2} & \text{if } p = 0, \\ a_{\frac{p+1}{2}} & \text{if } p \text{ is odd}, \\ b_{\frac{p}{2}} & \text{if } p \text{ is even}, \end{cases} \qquad \phi_p = \begin{cases} -\frac{\pi}{2} & \text{if } p \text{ is odd}, \\ 0 & \text{if } p \text{ is even}, \end{cases} \tag{9}$$

and

$$\xi_p = \frac{n(p)}{2\pi R} = \begin{cases} \frac{p+1}{4\pi R} & \text{if } p \text{ is odd}, \\ \frac{p}{4\pi R} & \text{if } p \text{ is even}. \end{cases} \tag{10}$$

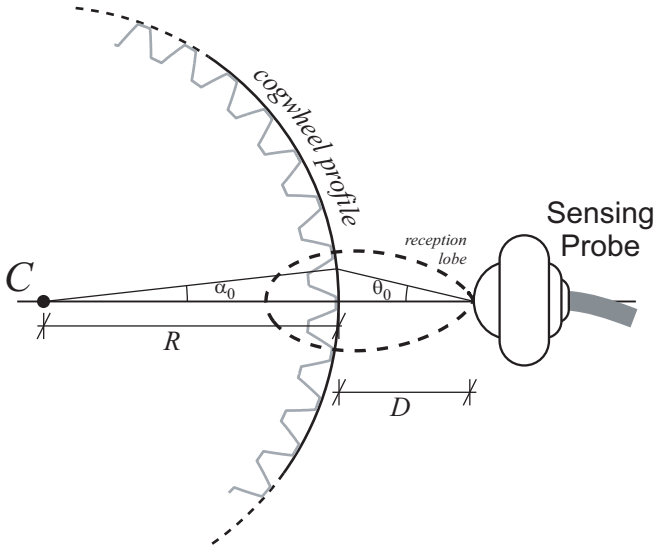


Figure 2: The probe spatial reception lobe is assumed to be focused on a small, limited portion of the cogwheel profile.

As a result, according to the above discussed approach, the rotational motion of the cogwheel in front of the probe can be equivalently described as a translation of the probe along the y-axis, in front of the unrolled periodic profile r_y.

3.1 Effects of the finite spatial accuracy of the probe

Due to the finite spatial accuracy of the probe, the actual detected profile height is determined by the convolution of the cogwheel 'unrolled' profile r_y with the projection of the spatial reception lobe (3) on the y-axis, i.e., with

$$f_y(y) = \sqrt{\frac{\ln 2}{\pi\theta_0^2}} e^{-\frac{\operatorname{arctg}^2 \frac{y}{D} \ln\sqrt{2}}{\theta_0^2}} \approx \sqrt{\frac{\ln 2}{\pi\theta_0^2}} e^{-\frac{y^2 \ln\sqrt{2}}{D^2\theta_0^2}}. \tag{11}$$

Since the above approximation holds when $\frac{y}{D}$ is small, eq. (11) has a practical validity when both θ_0 and D are reasonably small (i.e., the probe has an acceptable directivity, and it is positioned close to the cogwheel).

As a result, the profile detected by the probe is

$$\begin{aligned} r'_y(y) &\approx \int_{-\infty}^{+\infty} r_y(s) f_y(y-s)\, ds \approx \\ &\approx \sum_{p=0}^{\infty} \int_{-\infty}^{+\infty} A_p \cos(2\pi\xi_p\ s + \phi_p) e^{-\frac{(y-s)^2 \ln\sqrt{2}}{D^2\theta_0^2}} ds. \end{aligned} \tag{12}$$

The above sum of integrals can be suitably solved using Fourier transforms, recalling the transformation

$$e^{-ax^2} \overset{\mathcal{F}}{\Longleftrightarrow} \sqrt{\frac{\pi}{a}} e^{-\frac{(\pi\nu)^2}{a}}. \tag{13}$$

Accordingly, eq. (12) can be rewritten as

$$r'_y(y) \approx \sum_{p=0}^{\infty} A'_p \cos(2\pi\xi_p\ y + \phi_p), \tag{14}$$

where

$$A'_p = A_p\ e^{-\frac{(\pi\xi_p D\theta_0)^2}{\ln\sqrt{2}}}. \tag{15}$$

3.2 The probe output voltage signal

Using the above results the probe output voltage can be found relating the spatial variable y to the time, by means of the cogwheel angular velocity. Since the shaft rotational angle α is linked to the instantaneous angular velocity by an integral relationship, it results

$$\begin{aligned} y(t) = R\alpha(t) = R\alpha(0) + R\int_0^t \omega(\tau)d\tau = \\ = R\alpha(0) + R\omega_0 t + R\int_0^t \tilde{\omega}(\tau)d\tau. \end{aligned} \tag{16}$$

Substituting (16) in (14), by properly setting $\alpha(0) = 0$ without loss of generality, the following expression can be obtained

$$r'_y(t) \approx \sum_{p=0}^{\infty} A'_p \cos\left[2\pi\xi_p\left(R\omega_0 t + R\int_0^t \tilde{\omega}(\tau)d\tau\right) + \phi_p\right]. \tag{17}$$

The above summation describes the cogwheel profile detected by the probe, as a function of the time t. In other words, since the cogwheel rotation with respect to the probe is represented as a relative motion of the probe in front of the unrolled cogwheel profile, eq. (17) describes the height of the detected profile sampled in front of the probe, assuming the probe translating along the y-axis, according to (16).

The probe voltage V_{in} of Fig.1 can be finally determined by filtering the signal (17) with the probe electric response (4). At a first approximation the probe transfer function (4) is assumed to be constant over small disjoint bandwidths containing the frequency spectrum of each term in the summation (17) (this aspect is made clearer in Sec.4). As a result, the filtering of (17) with (4) changes the amplitudes A'_p and phases ϕ'_p in A''_p and ϕ''_p, respectively, obtaining

$$V_{in}(t) \approx \sum_{p=0}^{\infty} A''_p \cos\left[2\pi\xi_p\left(R\omega_0 t + R\int_0^t \tilde{\omega}(\tau)d\tau\right) + \phi''_p\right]. \tag{18}$$

Recalling def. (10), the authors emphasize that each term in the above summation represents the expression of *the classical frequency modulation* of sinusoidal carriers [11] with fundamental frequencies

$$f_{c,p} = R\xi_p\omega_0 = \frac{n(p)\omega_0}{2\pi}, n(p) \in \mathbb{N} \tag{19}$$

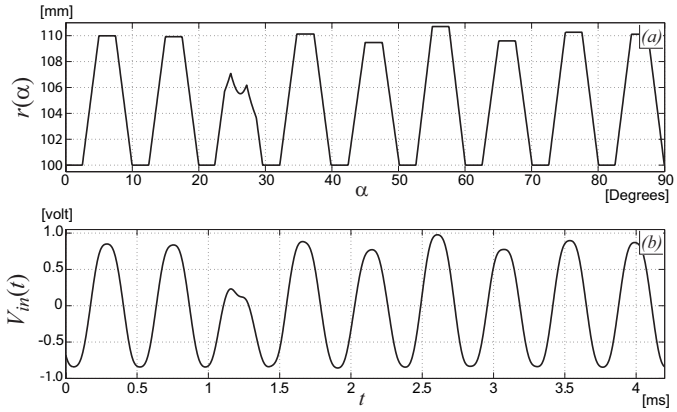


Figure 3: The effect of the finite resolution of the sensing probe on the first 90 degrees of the sensed rotating cogwheel profile: (a) cogwheel profile with irregular cogs; (b) correspondent normalized probe output voltage.

Accordingly, each term in the summation can be rewritten in the form

$$A\cos\left(n\omega_0 t + n\Delta\omega_{\max}\int_0^t m(\tau)d\tau + \phi\right). \tag{20}$$

These latter considerations will be made clearer in the next Sections.

Example 1

Let us consider a shaft rotating at $\omega_0 = 2\pi f_0 = 3600$ rpm, i.e., $f_0 = 60$ Hz (no angular vibrations). The used cogwheel has a nominal radius of 10 cm, an irregular profile ($N = 36$ trapezoidal cogs, with 0.5 mm of standard deviation in the mechanical profile, one broken cog). The nominal distance of the sensing probe is 10 mm, with 3 dB half-angle equal to 5° and pass-band cut-off frequencies $f_L = 2$ Hz and $f_H = 10$ kHz. As it can be seen in Fig. 3, due to the probe finite resolution the output voltage V_{in} expressed by (18) with $\tilde{\omega} = 0$, normalized to its maximum amplitude, describes a much smoother version of the unrolled cogwheel profile.

The signal V_{in} is periodic with period $T_0 = 1/60$ s, and it can be expressed as a Fourier series in which the terms of the form (20) have a frequency multiple of 60 Hz. The Fourier coefficients associated with those components corresponding to the 99.99% of the signal power are graphically represented in Fig. 4, where the a_n coefficients are related to cosines, and b_n coefficients are related to sines. As expected, most of the signal power is brought by those components at $n = 36$, that is equal to the number N of cogs in the wheel. These main components are associated to a major peak in the spectrum of V_{in}, at frequency $60 \cdot 36 = 2160$ Hz (Fig. 5). The other minor peaks are associated to the harmonic components of the Fourier expansion bringing the remaining part of the signal power, associated with the cogwheel imperfections.

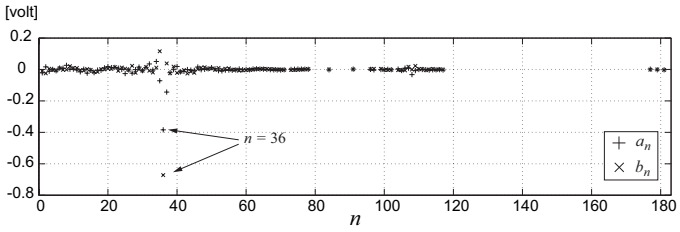


Figure 4: The Fourier coefficients associated to those components of (18) expressing the 99.99% of the signal power in the Example 1.

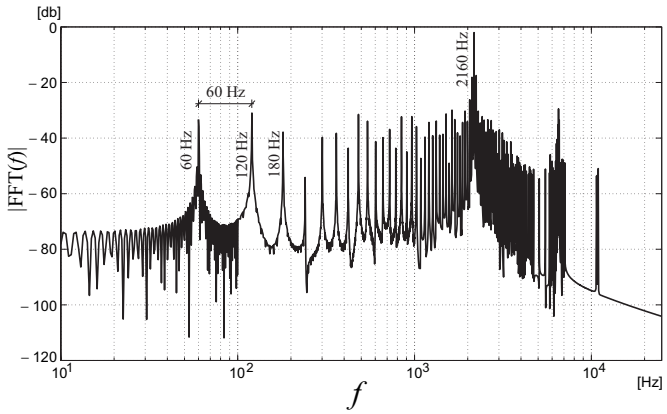


Figure 5: The spectrum of the signal V_{in} for the Example 1 (no angular vibrations of the rotating shaft). The harmonic components are related to the Fourier coefficients of Fig. 4

4 Probe signal spectrum: effects of the irregular cogwheel shape profile

Recalling the expression (18) that describes the output probe voltage, let us focus on a single term of the form (20). From a theoretical point of view, as it is well known, the frequency spectrum of a frequency-modulated signal has components extending out to infinite frequencies, although most of the signal power is spread around the carrier frequency. In this case, as it can be easily verified, the spectrum associated to each modulated component depends on both $n\Delta\omega_{\max}$ and the bandwidth W of the vibrational signal m. There are several methods to estimate the resulting bandwidth, among which a well known one is the *Carson bandwidth rule*, that states, to a first approximation [11],

$$B_n \approx \frac{n\Delta\omega_{\max}}{\pi} + 2W. \tag{21}$$

It is interesting noting that the carrier frequencies in (20) are equally spaced by $\frac{\omega_0}{2\pi}$ hertz, corresponding to the available bandwidth to avoid mutual interference between neighboring modulated carriers. In other words, referring to the Carson rule, it should result

$$\frac{n\Delta\omega_{\max}}{\pi} + 2W < \frac{\omega_0}{2\pi}. \tag{22}$$

Obviously, the spectrum of the n-th modulated carrier in (20) is affected by the interferences induced by the spectrum of the neighboring modulated carriers, *weighted by their powers*. As a result, for a perfectly sinusoidal-shaped cogwheel, the above interference problem would not exist, since in that case the Fourier series (7) would have only one component at spatial frequency $\frac{N}{2\pi R}$, being N the number of cogs.

Example 2

Let us consider the rotating shaft introduced in the Example 1, and let us introduce a single vibration tone of the angular velocity, referring to a vibrational phasor with angle $\tilde{\alpha} = \alpha_v \sin(2\pi f_v t)$ rad. Since $\tilde{\omega} = \frac{d}{dt}\tilde{\alpha}$, it results $\tilde{\omega}(t) = 2\pi f_v \alpha_v \cos(2\pi f_v t)$, and substituting in (22) $W = f_v$ and $\Delta\omega_{\max} = 2\pi f_v \alpha_v$, the inequality $2nf_v\alpha_v + 2f_v < f_0$ can be obtained, i.e.,

$$f_v < \frac{f_0}{2(n\alpha_v + 1)}. \tag{23}$$

Since most of the signal power is brought by the frequency component related to the number of cogs in the wheel (i.e., the modulated carrier at frequency Nf_0), the above inequality can be solved for $n = N = 36$, obtaining Fig. 6.

From the ineq. (23) it can be noticed that the problem of mutual interferences between modulated carriers strongly depends on the number of cogwheel cogs and on the rotating frequency of the shaft. More in general, when the vibrational motion is composed by more than one tone, the condition of mutual interference between modulated carriers is verified in most practical cases, when using cogwheels with not-regular profiles. This aspect must be taken into account when designing demodulating methods for the considered application, as discussed in Sec. 6.

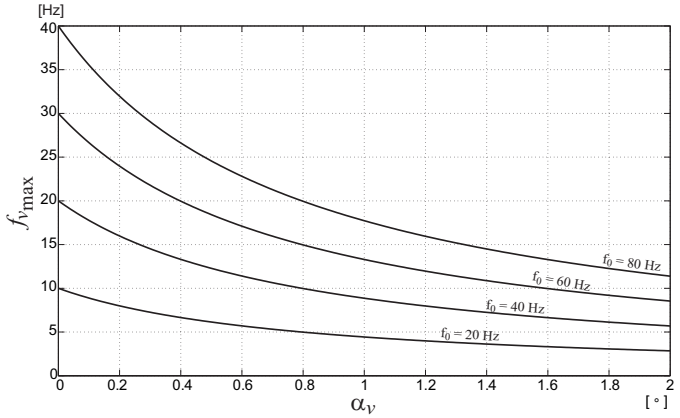


Figure 6: Maximum frequency of the vibrational tone for different vibrational angles and rotational speeds, to avoid mutual interferences between the modulated carriers (20), according to the Carson rule.

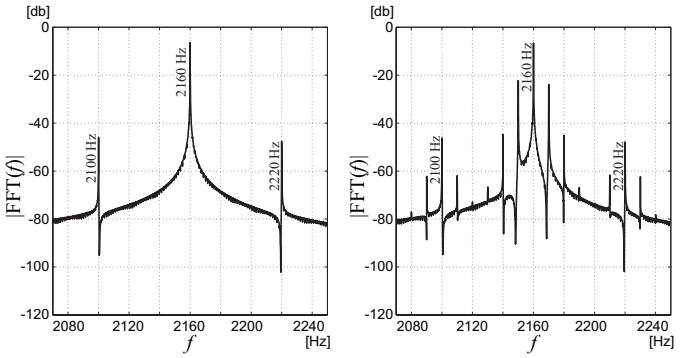


Figure 7: Portion of the frequency spectrum for the same signal V_{in} discussed in the Example 2, without vibration (left) and with vibration (right), assuming $\alpha_v = 0.5°$ and $f_v = 10$ Hz.

5 Effects of the shaft side vibrations

The shaft side vibrations are described by the motion of the cogwheel center **C** on the plane $x - y$. The effects on the probe signal frequency spectrum can be analyzed separating the two components along the different axes.

5.1 Side vibrations along the y-axis

In such case the eq. (16) must be rewritten as (the offset angle $\alpha(0)$ is set equal to 0)

$$\begin{aligned} y(t) = R\omega_0 t + R\int_0^t \tilde{\omega}(\tau)d\tau + C_y(t) = \\ = R\omega_0 t + R\int_0^t \left(\tilde{\omega}(\tau) + \frac{1}{R}\frac{d}{d\tau}C_y(\tau)\right)d\tau + C_y(0). \end{aligned} \tag{24}$$

It is interesting noting that the time derivative of the y-side vibrations determines a direct deterioration of the vibrational signal, inversely proportional to the cogwheel radius R.

5.2 Side vibrations along the x-axis

The side vibrations of the rotating shaft along the x-axis change the profile height of the cogwheel detected by the probe. In other words, the signal C_x must be added directly to the second member of eq. (7). From a qualitative point of view, the effect of these side vibrations introduces a factor of the form $(1 + S_x(t))$ modulating the amplitude of the signal V_{in}, where the signal S_x is obtained by taking into account of the probe filtering during each phase discussed before. The analytical relationship between $S_x(t)$ and C_x can not be expressed explicitly, in general. Nevertheless, in the following Sections, the authors will discuss how this aspect influences the estimation of the vibrational signal $\tilde{\omega}$.

6 The Vibrational Signal Estimation

In the previous sections it was shown how the frequency spectrum of the output voltage probe signal V_{in} is affected by the main non-idealities of the measuring set-up. At the same time, the authors have shown that the probe signal, beside the effects of the shaft side vibrations along the x-axis, can be represented by the infinite sums of frequency-modulated sinusoidal carriers at different frequencies multiple of f_0. In the case of a cogwheel with an ideal sinusoidal profile, eq. (18) reduces to a single frequency-modulated sinusoidal tone at center frequency Nf_0.

From a theoretical point of view, in order to retrieve the vibrational signal $\tilde{\omega}$ from V_{in}, classical FM demodulation methods represent good candidates to accomplish the task [11]. Nevertheless, the authors emphasize that there are several impediments to the implementation of most of the traditional methods, as discussed in the following. First of all, the considered application operates at extremely low frequencies, if compared to the classical FM modulation in telecommunications. Accordingly, the physical realization of band-pass filters to

select only that part of frequency spectrum interested by the main modulated carrier at frequency Nf_0 is highly critical (also considering that the rotating shaft f_0 is unknown a priori). Moreover, the authors have shown in Sec. 4 that neighbor modulated carriers can introduce mutual interferences, depending on the deviation ratio $\Delta\omega_{\max}/2\pi W$.

As discussed in the introduction, in this paper the authors show that a simple variant of the well known zero-crossing frequency demodulation method can represent a valid solution to measure the vibrational signal $\tilde{\omega}$, suitable for the kind of considered applications. Differently from the classical approach in which the zero-crossing demodulation is applied to a single frequency-modulated sinusoidal carrier, the method is directly applied to the probe signal V_{in}, *without any preliminary filtering*, proposing measurement methods combining the signals of more than one probe to reject the effects of the shaft side vibrations or of the non-regular cogwheel shape profile.

6.1 The zero-crossing method

The classical zero crossing demodulation method is defined assuming the signal V_{in} to be a single frequency modulated cosine at frequency Nf_0, according to the form (20) [11–13]. Every time the signal V_{in} is equal to zero the argument of the cosine function is equal to $\frac{\pi}{2} + k\pi$, with $k \in \mathbb{Z}$. By simply measuring the time between two consecutive zeros, i.e., t_n and t_{n+1}, it results

$$2\pi N f_0(t_{n+1} - t_n) + N \int_{t_n}^{t_{n+1}} \tilde{\omega}(\tau)d\tau = \pi. \tag{25}$$

Using the integral mean value theorem, assuming $\tilde{\omega}$ to be continuous, there exists $\tau_n \in [t_n, t_{n+1})$ such that $\int_{t_n}^{t_{n+1}} \tilde{\omega}(\tau)d\tau = (t_{n+1} - t_n)\tilde{\omega}(\tau_n)$. Accordingly, by defining $\Delta t_n = t_{n+1} - t_n$, eq. (25) becomes

$$\Delta t_n(N\omega_0 + N\tilde{\omega}(\tau_n)) = \pi \Longrightarrow \omega(\tau_n) = \frac{\pi}{N\Delta t_n}. \tag{26}$$

In other words, assuming $\tilde{\omega}$ to vary slowly with respect to Δt_n, the above result provides a direct estimation of the instantaneous angular velocity ω at the time t_n, i.e.,

$$\omega(t_n) \approx \frac{\pi}{N\Delta t_n}. \tag{27}$$

From the above estimation, one can estimate the mean value ω_0 and then the vibrational part $\tilde{\omega}$, using eq. (1).

In this case, the signal V_{in} (18) is *not* a simple FM signal and some precautions must be taken into account, as discussed in the following. First of all, it can be noted that in (27) the angle π/N is equal to half of the average angle subtended by a cog to the cogwheel center. In other words, since (27) was derived assuming the signal to be a FM modulated carrier with frequency Nf_0, the instantaneous angular velocity is simply estimated dividing half the angle subtended by a cog by the time the shaft takes to rotate by this angle. As it is known, the cogs can be different from each others, therefore the actual angle subtended between two zero-crossing times have to be modeled as a random variable φ.

6.2 Sensitivity analysis

On the basis of (27), the estimation $\hat{\omega}$ of the instantaneous angular velocity can be written as a function of two random variables φ and Δt, i.e.,

$$\hat{\omega} = \frac{\varphi}{\Delta t}. \tag{28}$$

The random variable Δt represents the measured value $t_{n+1} - t_n$, as obtained from the signal processing involved by the zero-crossing technique, and its random fluctuations account for the measurement errors. On the other hand, φ represents the rotation angle covered by the shaft during the time Δt. It is a random variable since in the estimation (27) this angle is assumed to be equal to $\frac{\pi}{N}$, whereas its actual value is affected by the irregular cogwheel profile.

By denoting with φ_0 and Δt_0 the mean values of φ and Δt, in the following the authors define $\varphi = \varphi_0 + \delta\varphi$ and $\Delta t = \Delta t_0 + \delta t$, where $\delta\varphi$ and δt represents the zero-mean fluctuations of φ and Δt around φ_0 and Δt_0, respectively. Accordingly, the def. (28) can be rewritten referring to its first order Taylor expansion

$$\begin{aligned} \hat{\omega}|_{\varphi_0,\Delta t_0} &\approx \\ \approx \frac{\varphi_0}{\Delta t_0} + \frac{\partial\hat{\omega}}{\partial\varphi}(\varphi_0,\Delta t_0)\delta\varphi + \frac{\partial\hat{\omega}}{\partial\Delta t}(\varphi_0,\Delta t_0)\delta t &= \\ = \frac{\varphi_0}{\Delta t_0} + \frac{1}{\Delta t_0}\delta\varphi - \frac{\varphi_0}{\Delta t_0^2}\delta t. & \end{aligned} \tag{29}$$

From a statistical point of view, the random variable $\hat{\omega}$ has mean value

$$\mu_{\hat{\omega}} = E\{\hat{\omega}\} \approx \frac{\varphi_0}{\Delta t_0}, \tag{30}$$

and variance

$$\begin{aligned} \sigma^2_{\hat{\omega}} &= E\{(\hat{\omega} - \mu_{\hat{\omega}})^2\} \approx \\ \approx \frac{1}{\Delta t_0^2}\sigma^2_{\varphi} + \frac{\varphi_0^2}{\Delta t_0^4}\sigma^2_{\Delta t} - \frac{2\varphi_0}{\Delta t_0^3}E\{\delta\varphi\ \delta t\}, & \end{aligned} \tag{31}$$

where $\sigma^2_{\Delta t}$ and σ^2_{φ} are the variances of Δt and φ, respectively.

It is worth noting that the third term in the above expression would be zero if Δt and φ were statistically independent: that is not true since the zero-crossing times are correlated to the actual angles subtended by the cogs. In the worst case, by assuming a correlation coefficient $\rho = -1$ between Δt and φ, the above result can be limited by the upper-bound

$$\begin{aligned} \sigma^2_{\hat{\omega}} \leq \frac{1}{\Delta t_0^2}\sigma^2_{\varphi} + \frac{\varphi_0^2}{\Delta t_0^4}\sigma^2_{\Delta t} + \frac{2\varphi_0}{\Delta t_0^3}\sigma_{\varphi}\sigma^2_{\Delta t} &= \\ = \frac{1}{\Delta t_0^2}\left(\sigma_{\varphi} + \frac{\varphi_0}{\Delta t_0}\sigma_{\Delta t}\right)^2. & \end{aligned} \tag{32}$$

The square root of (31) or, equivalently, the square root of the right side of (32), describes the uncertainty about the estimation of the instantaneous angular velocity of the rotating shaft. About this point, it can be noted that

as a general trend the variance $\sigma^2_{\hat{\omega}}$ is heavily affected by $\sigma^2_{\Delta t}$ as far as Δt tends to zero. This may happen, referring to the case considered in this work, if for a fixed cogwheel the shaft rotating frequency goes to infinity ($\omega_0 \to \infty$) or, for a shaft rotating at constant speed, if $\varphi \to 0$ (i.e., the number of cogs $N \to \infty$).

The above theoretical results have general validity if the higher order terms in the Taylor expansion of (28) are negligible, e.g.,

$$\begin{aligned} \frac{1}{10}\left|\frac{\partial\hat{\omega}_\varphi}{\partial\varphi}\delta\varphi + \frac{\partial\hat{\omega}}{\partial\Delta t}\delta t\right| < \\ \frac{1}{2}\left|\frac{\partial^2\hat{\omega}}{\partial\varphi^2}\delta\varphi^2 + \frac{\partial^2\hat{\omega}}{\partial\Delta t^2}\delta t^2 + \frac{\partial^2\hat{\omega}}{\partial\varphi\partial\Delta t}2\delta t\ \delta\varphi + \right|, \end{aligned} \tag{33}$$

that is

$$\frac{1}{10}\left|\frac{1}{\Delta t_0}\delta\varphi - \frac{\varphi_0}{\Delta t_0^2}\delta t\right| < \left|\frac{\varphi_0}{\Delta t_0^3}\delta t^2 - \frac{1}{\Delta t_0^2}\delta t\ \delta\varphi\right|. \tag{34}$$

6.3 Simplified analysis

It can be easily shown that the random variable φ has mean value $\varphi_0 = \frac{\pi}{N}$ and $\delta\varphi \neq 0$ if and only if the cogwheel does not have N equal cogs.

Nevertheless, from a statistical point of view any uncertainty about the angle φ can be expressed as an uncertainty about the time Δt. This approach is founded on the deterministic integral equation

$$\varphi = \int_{\Delta t} \omega(\tau) d\tau, \tag{35}$$

that links the actual values of Δt and φ. Accordingly, even for a not-ideal cogwheel, the quantity $\varphi = \frac{\pi}{N}$ can be assumed constant, being the stochastic part δt as the sum of two statistically independent quantities

$$\delta t = \delta t_\varphi + \delta t_m, \tag{36}$$

where δt_φ is the random fluctuation associated to the (actually random) angle φ and δt_m is the uncertainty related to the measure of Δt. Referring to the above theoretical model, the equations (29)-(34) can be simplified as in the following:

$$\hat{\omega}|_{\varphi_0,\Delta t_0} \approx \frac{\pi}{N\Delta t_0}\left(1 - \frac{\delta t}{\Delta t_0}\right), \tag{37}$$

$$\mu_{\hat{\omega}} \approx \frac{\pi}{N\Delta t_0}, \tag{38}$$

and variance

$$\sigma^2_{\hat{\omega}} \approx \frac{\pi^2}{N^2\Delta t_0^4}\sigma^2_{\Delta t}. \tag{39}$$

The variance $\sigma^2_{\Delta t}$ can be expressed recalling (36) and the statistical independence of δt_m and δt_φ, obtaining

$$\sigma^2_{\Delta t} = E\{\delta t_m^2\} + E\{\delta t_\varphi^2\}. \tag{40}$$

Assuming the shaft angular velocity ω to be greater than a minimum value $\omega_{\min}$ and, to a first approximation, assuming ω to be constant within the time interval Δt, the second term at the right side of (40) can be written as

$$E\{\delta t_\varphi^2\} \approx E\left\{\left(\frac{\delta\varphi}{\omega}\right)^2\right\} < \frac{\sigma_\varphi^2}{\omega_{\min}^2}. \tag{41}$$

Accordingly, by denoting with $\sigma_{\Delta t_m}^2$ the variance of the error in the measurement of the time-interval Δt, combining the above results from eq. (39) the following expression can be obtained

$$\sigma_{\hat{\omega}}^2 < \frac{\pi^2}{N^2 \Delta t_0^4}\left(\sigma_{\Delta t_m}^2 + \frac{\sigma_\varphi^2}{\omega_{\min}^2}\right). \tag{42}$$

Finally, by noting that

$$\Delta t_0 = \frac{1}{2Nf_0}, \tag{43}$$

it is possible to express the uncertainty about the estimation of $\hat{\omega}$ as

$$\begin{aligned} u(\hat{\omega}) &\approx \frac{\pi}{N\Delta t_0^2}\sigma_{\Delta t} = 4\pi N f_0^2 \sigma_{\Delta t} = \\ &= \frac{N\omega_0^2}{\pi}\sigma_{\Delta t} < \frac{N\omega_0^2}{\pi}\sqrt{\sigma_{\Delta t_m}^2 + \frac{\sigma_\varphi^2}{\omega_{\min}^2}}. \end{aligned} \tag{44}$$

The above theoretical results have general validity if the higher order terms in the Taylor expansion of (28) are negligible, e.g., combining (43) with (34),

$$\delta t < \frac{\Delta t_0}{10} = \frac{1}{20Nf_0}. \tag{45}$$

Summarizing, eq. (44) characterizes the resolution of the measurement set-up, as clarified also by the following example. As a general comment, the authors emphasize that the higher is (44), and the lower is the quality of the estimated signal ω used for retrieving the vibrational signal $\tilde{\omega}$, according to (1).

Example 3

Let us consider the cogwheel of the Example 1, rotating at 3600 rpm, i.e., $f_0 =$ 60 Hz. Assuming small vibrations of ω around ω_0, in order to have a relative rms error lower than 0.5% in the measurement of the instantaneous angular velocity, from (44) it results

$$4\pi N f_0^2 \sigma_{\Delta t} < \frac{0.5}{100}\, 2\pi f_0, \tag{46}$$

that implies, recalling that $N = 36$, $f_0 = 60$ Hz,

$$\sigma_{\Delta t} < \frac{5}{1000\ 2Nf_0} \approx 1.16\ \mu\text{s}. \tag{47}$$

The upper-bound is meaningful since (45) is satisfied.

It is worth noting that the maximum rms for the measurement of Δt found in (47) includes the *cumulative effects of the measurement set-up non-idealities*, i.e., the induced effects of the shaft side vibrations and of the irregular cogwheel shape profile.

On the other hand, ineq. (44) can be used to estimate an upper-bound for the uncertainty in the measurement of ω. For example, let us assume for the zero-crossing method a time-measurement accuracy $\delta_{t_m} = 1$ μs. Moreover, if for the cogwheel of radius $R = 100$ mm a mechanical standard deviation of the cogs size of 0.5 mm is assumed, it results $\sigma_\varphi \approx \frac{0.5}{100} = 5 \cdot 10^{-3}$ rad. Furthermore, if the lower shaft rotation frequency is assumed to be greater than 55 Hz, from ineq. (44) it can be obtained

$$\begin{gathered} \frac{u(\hat{\omega})}{2\pi f_0} = 2N f_0 \sigma_{\Delta t} < \\ 2 \cdot 36 \cdot 60 \cdot \sqrt{10^{-12} + \frac{25 \cdot 10^{-6}}{4\pi^2 55^2}} \approx 0.62\%, \end{gathered} \tag{48}$$

that is, a relative rms error in the estimation of the instantaneous angular velocity not greater than 0.62%.

This example reveals that in order to achieve high measurement resolutions, sophisticated measurement set-up should be mandatory, i.e., a cogwheel with an almost perfect shape profile and negligible shaft side vibrations. Nevertheless, as discussed in the following sections, methods to reject the effects of the non-idealities can increase considerably the resolution of the measurement, even considering badly shaped cogwheels.

7 Rejection of the irregular cogwheel shape

According to the above discussion, the effects of the irregular cogwheel shape on the measurement can be taken into account assuming the cogwheel to be perfectly shaped and introducing an equivalent error in the estimation of the zero-crossing times. For the moment, let us analyze the case of a shaft rotating with no side vibrations and let us assume the uncertainty δt_m in (36) to be equal to zero. Since the authors are applying the zero-crossing demodulation method to the unfiltered signal V_{in}, they account for the cogwheel irregularities introducing a phase-error in (25), i.e.,

$$2\pi N f_0 (t_{n+1} - t_n) + N \int_{t_n}^{t_{n+1}} \left(\tilde{\omega}(\tau) + \frac{d}{d\tau}\zeta(\tau) \right) d\tau = \pi. \tag{49}$$

Due to the periodicity of the cogwheel shape (each cog is periodic with periodic angle 2π), the signal ζ is strictly linked to $\omega = \omega_0 + \tilde{\omega}$. Nevertheless, once referring to small vibrations with vibration frequency quite smaller than $N f_0$, to a first approximation ζ can be assumed to have period $T_0 = \frac{1}{f_0}$. Under this hypothesis, the demodulated signal is

$$\hat{\omega} \approx \omega_0 + \tilde{\omega} + \frac{d}{d\tau}\zeta. \tag{50}$$

The third term on the right side of (50) is periodic with period T_0, and this fact introduces in the frequency spectrum of $\hat{\omega}$ a sequence of spurious harmonics at

multiple frequencies of f_0. In the following, the authors theoretically discuss a method to reject these spurious harmonics.

7.1 Signals with periodic noisy components

Let us consider the periodic signal $Z = \frac{d}{dt}\zeta$ with period T_0. It can be easily proved the following

Proposition 1 *The signal*

$$\Upsilon(t) = \sum_{i=1}^{M} Z\left(t - (i-1)\frac{T_0}{M}\right) \tag{51}$$

has period $\frac{T_0}{M}$*, for* $M \in \mathbb{N}$*,* $M > 0$*.*

Proof. It results

$$\begin{aligned} \Upsilon\left(t + \frac{T_0}{M}\right) &= \sum_{i=1}^{M} Z\left(t - i\frac{T_0}{M}\right) = \\ &= \sum_{i=2}^{M} Z\left(t - (i-1)\frac{T_0}{M}\right) + Z(t+T_0) = \Upsilon(t). \end{aligned} \tag{52}$$

□

It is interesting noting that the frequency spectrum of Υ contains a sequence of spurious harmonics at frequencies multiple of Mf_0. In other words, the frequency spectrum of Υ is empty between 0 Hz and Mf_0.

7.2 A measurement set-up using more than one probe

From the previous discussion, the authors recall that the phase error introduced by the cogwheel irregularities $\frac{d}{d\tau}\zeta$ is periodic with period T_0. Accordingly, the above theoretical result can be used to define a measurement set-up based on $M > 1$ probes: the probes have to be placed at different positions around the cogwheel, such to obtain a phase difference between the noisy electrical components introduced by the cogwheel irregularities. Indeed, taking as a reference the first probe at angle position 0° (as in Fig. 1), the electric signal issued by the i-th probe placed at the angle α_i is,

$$\begin{aligned} V_{in_i}(t) \approx \sum_{p=0}^{\infty} A''_p \cos\Bigg(n(p)\omega_0 t + \\ + n(p)\int_0^t \left[\tilde{\omega}(\tau) + \frac{d}{d\tau}\zeta\left(\tau - \frac{\alpha_i}{2\pi}T_0\right)\right] d\tau + \phi''_p\Bigg), \end{aligned} \tag{53}$$

where (18) and (19) were combined. As a result, averaging the demodulated signals obtained applying the zero-crossing method to each probe voltage, it results

$$\begin{aligned} \hat{\omega}_M(t) &\approx \frac{\sum_{i=1}^{M} \omega_0 + \tilde{\omega}(t) + \frac{d}{d\tau}\zeta\left(\tau - \frac{\alpha_i}{2\pi}T_0\right)}{M} = \\ &= \omega_0 + \tilde{\omega}(t) + \frac{1}{M}\sum_{i=1}^{M} \frac{d}{d\tau}\zeta\left(\tau - \frac{\alpha_i}{2\pi}T_0\right). \end{aligned} \tag{54}$$

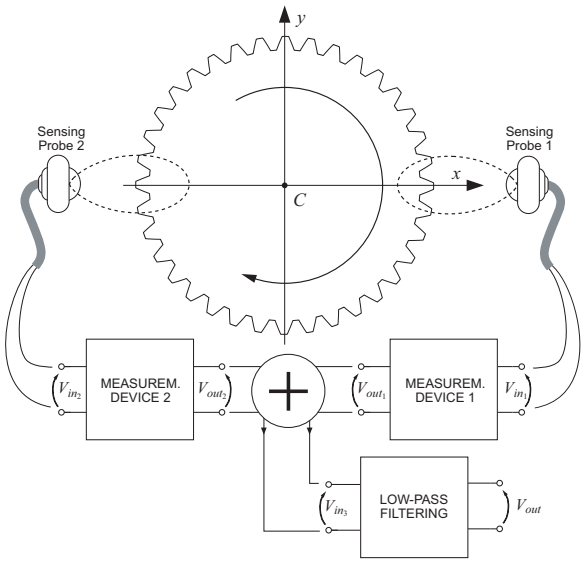


Figure 8: The simplest configuration to reject the effects induced at low-frequencies by the irregular cogwheel shape profile. The configuration can be made more complicated, e.g., using three probes at $0°, 120°, 240°$.

If α_i is set equal to $\frac{2\pi(i-1)}{M}$, i.e., if the probes are uniformly distributed around the cogwheel, it results from Proposition 1 that the noisy harmonics introduced by the cogwheel irregular shape are moved to the frequencies multiple of Mf_0: by properly choosing the number of probes M, the noisy effects of the cogwheel irregularities can be eliminated by low-pass filtering. The authors underline that this result holds *regardless of the cogwheel shape profile*.

Example 4

Let us consider the cogwheel rotating at 60 Hz, introduced in the previous example, and let us assume the shaft angular velocity to vibrate around ω_0 according to two vibrational phasors with angles $\tilde{\alpha}_1 = 0.5° \sin(2\pi 10t)$ and $\tilde{\alpha}_2 = 0.5° \sin(2\pi 50t)$, respectively. According to what discussed in Section 4, a case exhibiting deep mutual interference between contiguous frequency modulated carriers is being analyzed. By applying the zero-crossing method discussed in Sec. 6.1 different results are obtained using one, two or three probes evenly distributed around the cogwheel. As it can be seen in Fig. 9 the irregular cogwheel shape profile introduces spurious harmonics at frequencies multiple of 60 Hz. Using two probes the harmonics are moved to higher frequencies, multiple of 120 Hz, whereas using three probes the remaining spurious harmonics are present at frequencies multiple of 180 Hz, as confirmed by the theoretical analysis discussed in this Section.

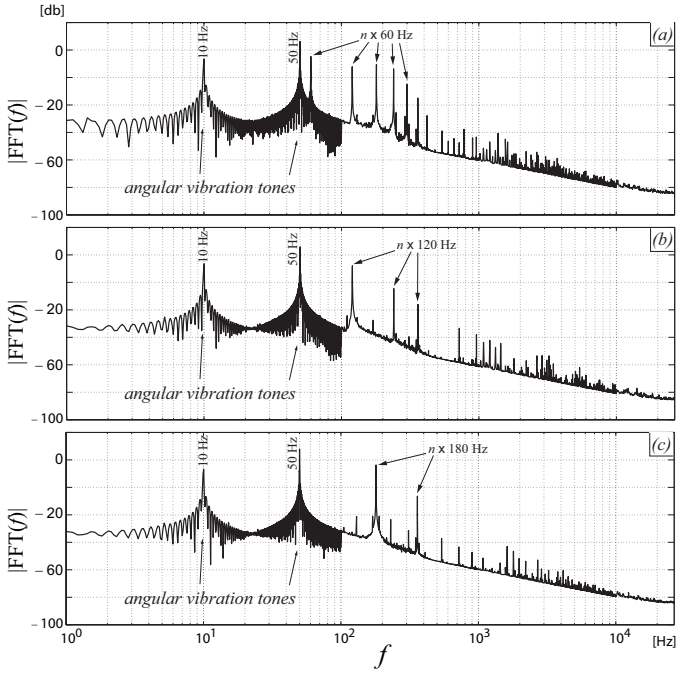


Figure 9: Frequency spectrum of the estimated angular vibration, obtained applying the zero-crossing method to the probe signals. From top to bottom: *(a)* one probe (0°), *(b)* two probes (0°, 180°), *(c)* three probes (0°, 120°, 240°).

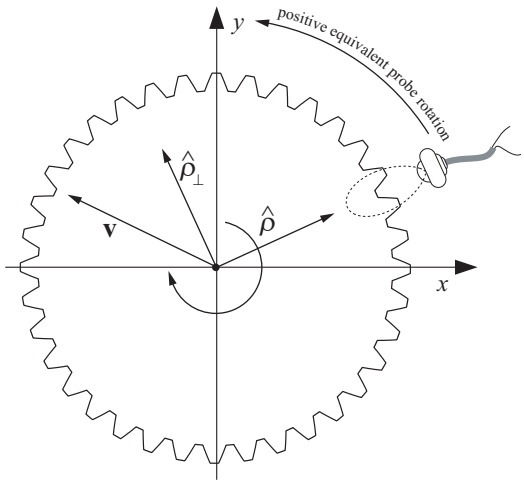


Figure 10: The geometric reference model for taking into account of the shaft side vibrations.

8 Rejection of the shaft side vibrations

In this section the authors refer to a generic probe positioned anywhere around the cogwheel, provided to have a symmetrical reception lobe (as in Fig. 1). As discussed in Sec. 5, small shaft side vibrations can be analyzed by splitting the cogwheel movements in components parallel and orthogonal to the probe.

In the following, the authors denote with $\hat{\rho}$ the radial unity vector identifying the nominal probe positioning angle, whereas $\mathbf{v}$ denotes the velocity vector of the cogwheel center, i.e., $\mathbf{v} = \frac{d\mathbf{C}}{dt}$. Referring to the Fig. 10, the parallel component $\mathbf{v}_{//}$ of $\mathbf{v}$ is determined by the scalar product between $\mathbf{v}$ and $\hat{\rho}$, that is

$$\mathbf{v}_{//} =< \mathbf{v} \cdot \hat{\rho} > \hat{\rho}, \tag{55}$$

whereas the orthogonal component $\mathbf{v}_\perp$ of $\mathbf{v}$ is

$$\mathbf{v}_\perp = \mathbf{v} - < \mathbf{v} \cdot \hat{\rho} > \hat{\rho}. \tag{56}$$

Equivalently, the latter quantity can be expressed referring to the orthogonal unity vector $\hat{\rho}_\perp$ represented in Fig.10, i.e., $\mathbf{v}_\perp =< \mathbf{v} \cdot \hat{\rho}_\perp > \hat{\rho}_\perp$.

From the probe point of view, the shaft side vibrations can be equivalently described as changes of the probe position in front of the cogwheel. In detail, a small movement of the cogwheel orthogonally to the probe can be described as a variation of the probe angle-positioning, that is equivalent to a variation of the cogwheel angular velocity given by

$$\Delta\omega_\perp \approx \frac{v_\perp}{R} = \frac{< \mathbf{v} \cdot \hat{\rho}_\perp >}{R}, \tag{57}$$

being R the cogwheel radius. On the other hand, a small side movement of the cogwheel parallel to the probe can be described as a variation of the probe distance from the shaft.

It is of interest to evaluate the overall effect of a cogwheel side movement when M measurements obtained using M probes are averaged as in Fig. 8. If $M > 1$ probes are evenly distributed around the cogwheel according to $\hat{\rho}_1, \ldots, \hat{\rho}_M$, it is easy to check that due to symmetry

$$\sum_{i=1}^{M} \hat{\rho}_i = \sum_{i=1}^{M} \hat{\rho}_{i_\perp} = 0. \tag{58}$$

Let us focus on the shaft side vibration components orthogonal to the probes. According to the proposed notation and assumptions (see Fig. 1), the positive direction of the shaft rotation is clockwise: in other words, if the cogwheel is locked and if the dynamics is described from the probes point of view, the positive direction of the probes rotation is counter-clockwise. Therefore, adopting the probe point of view to describe the dynamics, if $< \mathbf{v} \cdot \hat{\rho}_\perp >$ is negative the probe is rotating faster around the locked cogwheel. Accordingly, exploiting the symmetry of the setup (58), by averaging the equivalent angular velocity variations (57) detected by each probe it results

$$\begin{aligned} \frac{1}{M} \sum_{i=1}^{M} \Delta\omega_{i_\perp} &= \frac{1}{M} \sum_{i=1}^{M} \frac{< \mathbf{v} \cdot \hat{\rho}_{i_\perp} >}{R} = \\ &= \frac{1}{M} \frac{< \mathbf{v} \cdot \sum_{i=1}^{M} \hat{\rho}_{i_\perp} >}{R} = 0. \end{aligned} \tag{59}$$

In Subsec. 5.1 the authors have shown that the orthogonal components of the shaft side vibrations modify directly the angular vibrational signal, i.e., for each probe the zero-crossing method reveals the components $v_\perp$ of the shaft side vibrations. As a result, (59) indicates that when M measurements obtained using M probes are averaged as in Fig. 8, the overall effect introduced by the equivalent angular velocity variations $\Delta\omega_{i_\perp}$ is canceled, regardless of the direction and magnitude of $\mathbf{v}$.

On the other hand, let us now focus on the shaft side vibration components parallel to the probes. As discussed in the Subsec. 5.2, these side vibrations change the height of the cogwheel shape detected by the probes, introducing for each probe a different factor $(1 + S_{//}(t))$ modulating the amplitude of the signal V_{in}. The analytical relationship existing between the amplitude modulating factor and the result of the zero-crossing demodulation method depends on several parameters, among which the cogwheel shape. Nevertheless, adopting an heuristic approach and exploiting the symmetry of the setup (58), also in this case it results

$$\sum_{i=1}^{M} < \mathbf{v} \cdot \hat{\rho} > = < \mathbf{v} \cdot \sum_{i=1}^{M} \hat{\rho} > = 0, \tag{60}$$

that is, the average of the geometrical projection of the parallel cogwheel vibration components is canceled due to symmetry. Furthermore, referring to Fig. 11, for the aims of this paper it is sufficient to note that, as a general rule, if the continuous signal V_{in} is multiplied by $(1 + S_{//}(t))$ leads or lags of the zero-crossing times occurs, affecting the estimation of the instantaneous angular velocity. These zero-crossing times variations have opposite amplitudes for probes positioned at different side of the shaft. Finally, the authors remark that

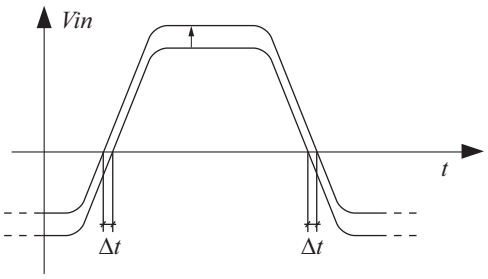


Figure 11: The effects of the amplitude modulation factor $(1 + S_{//}(t))$ on the zero-crossing times.

the zero-crossing technique is a FM demodulation operation, that is intrinsically robust to amplitude variations of the signal to be demodulated, as it is well know from telecommunication theory [11, 14].

As a result, as shown in the following example, when M measurements obtained using M probes are averaged as in Fig. 8, the overall effect of the shaft side vibrations is suitably rejected.

Example 5

Let us consider the same shaft of the previous example, rotating at 60 Hz. Two elliptical shaft side vibrations having 0.1 mm of major axis and frequency 60 Hz (1x) and 90 Hz (1.5x) are now introduced. By applying the zero-crossing method discussed in Sec. 6.1 different results are obtained using one or two probes. As it can be seen in Fig. 12 the irregular cogwheel shape profile introduces spurious harmonics at frequency multiples of 60 Hz, like in the previous example. Furthermore, when using a single probe the shaft side vibrations introduces two spurious harmonics at 60 Hz (mixed with the 60 Hz harmonic related to the irregular cogwheel shape), and at 90 Hz. By averaging the measurement of two probes (positioned at 0° and 180°), the shaft side vibrations were suitably rejected, whereas the odd harmonics at frequency multiples of 60 Hz were eliminated, as expected from the theory presented in Sec. 7. If using three probes, the results agree with the case *(c)* discussed in the Example 4, confirming that the shaft side vibrations are suitably rejected for $M > 1$. In Fig. 13 the authors reported the estimation of the shaft angular vibration versus time, for both of the considered cases (one or more probes), compared to the theoretical angular vibration signal. The time-delay between the theoretical angular vibration signal and the measurement signal is due to the FIR low-pass filtering at cut-off frequency of 100 Hz.

9 Conclusions

In this paper the authors have discussed a measurement method based on the zero-crossing demodulation technique of FM signals, to estimate the angular velocity vibrations of rotating shafts. The demodulation algorithm is applied without any filtering to the direct voltage output issued by one or more probes sensing the passages of some targets installed on the rotating shaft. The authors

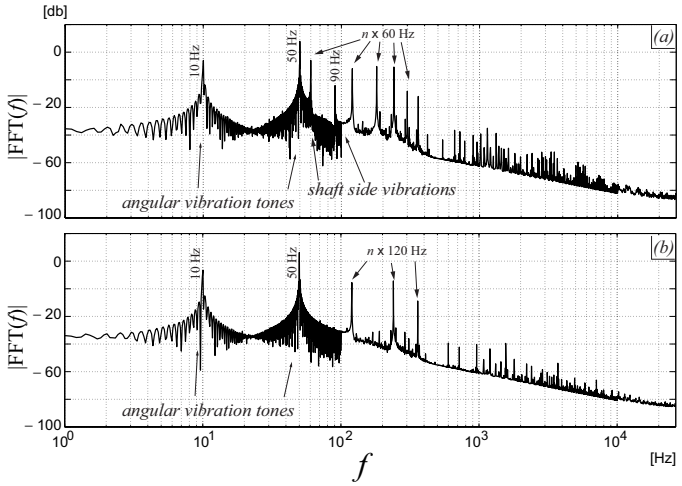


Figure 12: Frequency spectrum of the estimated angular vibration, obtained applying the zero-crossing method to the probe signals. From top to bottom: *(a)* one probe (0°), *(b)* two probes (0°, 180°). The shaft side vibrations have frequencies 60 Hz and 90 Hz.

have framed the measurement problem within a theoretical framework taking into account the chief non-idealities related to the measurement set-up, i.e., both the effects of the shaft side vibrations and the effects of the irregular target shapes are analyzed. The theoretical approach allowed to propose a measurement method that can suitably reject the effects of these mentioned non-idealities, based on the simple averaging of the measurement of two or more probes evenly positioned around the rotating shaft.

References

[1] L. Zhen, Z. An, and Q. Li, "Calculate engine crankshaft angular acceleration based on original flywheel data," in *Mechanic Automation and Control Engineering (MACE), 2010*, 2010, pp. 3141–3144.

[2] P. Wang, P. Davies, J. Starkey, and R. Routson, "A torsional vibration measurement system," in *Instrumentation and Measurement Technology Conference, 1992. IMTC '92., 9th IEEE*, 1992.

[3] ——, "A torsional vibration measurement system," *IEEE Transactions on Instrumentation and Measurement*, vol. 41, pp. 803 – 807, 1992.

[4] M. Lebold, K. Maynard, K. Reichard, M. Trethewey, J. Hasker, C. Lissenden, and D. Dobbins, "A non-intrusive technique for on-line shaft crack detection and tracking," in *Aerospace Conference, 2005 IEEE*, 2005.

[5] F. Yongqing and W. Kinsner, "A marine engine torsion vibration measuring method and its implementation based on fpga," in *Canadian Conference on Electrical and Computer Engineering, 2002. IEEE CCECE 2002.*, 2002.

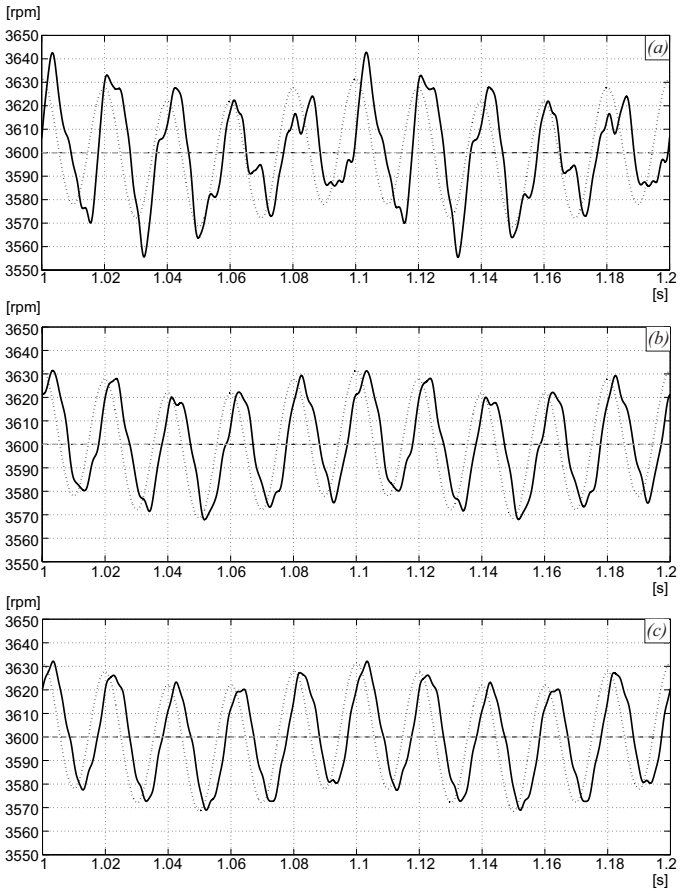


Figure 13: The estimation of the shaft angular vibration obtained using *(a)* one probe (0°), *(b)* two probes (0°, 180°) and *(c)* three probes (0°, 120°, 180°). The time-delay between the theoretical and the measurement signals is due to the FIR low-pass filtering at cut-off frequency of 100 Hz.

[6] F. C. Gómez de León and P. Meroño Pérez, "Discrete time interval measurement system: fundamentals, resolution and errors in the measurement of angular vibrations," *Measurement Science and Technology*, vol. 21, no. 7, July 2010.

[7] P. Sue, D. Wilson, L. Farr, and A. Kretschmar, "High precision torque measurement on a rotating load coupling for power generation operations," in *Instrumentation and Measurement Technology Conference (I2MTC), Graz (Austria)*, 2012, pp. 518–523.

[8] L. Naldi, R. Biondi, and V. Rossi, "Torsional vibrations in rotordynamic systems, identified by monitoring gearbox behaviour," in *Proceedings of the GT2008, ASME Turbo Expo*, 2008.

[9] L. Naldi, M. Golebiovski, and V. Rossi, "New approach to torsional vibration monitoring," in *Proceedings of the Fortieth Turbomachinery Symposium, Houston (Texas)*, 2011, pp. 60–71.

[10] T. Addabbo, R. Biondi, S. Cioncolini, A. Fort, M. Mugnaini, S. Rocchi, and V. Vignoli, "A multi-probe setup for the measurement of angular vibrations in a rotating shaft," in *Proceedings of the 2012 IEEE Sensors Applications Symposium, Brescia, Italy*, 2012.

[11] S. Haykin and M. Moher, *Introduction to analog and digital communications.* John Wiley 2007.

[12] R. Wiley, "Approximate FM demodulation using zero crossings," *IEEE Trans. on Communications*, vol. COM-29, no. 7, pp. 1061–1065, July 1981.

[13] H. Voelcker, "Zero-crossing properties of angle-modulated signals," *IEEE Trans. on Communications*, vol. COM-20, pp. 307–315, 1972.

[14] G. Kelley, "Choosing the optimum type of modulation–a comparison of several communication systems," *Communications Systems, IRE Transactions on*, vol. 6, no. 1, pp. 14–21, 1958.